PROCEEDINGS, Fire and Evacuation Modeling Technical Conference 2011
Baltimore, Maryland, August 15-16, 2011

QUALITY ASSESSMENT IN THE FIRE DYNAMICS SIMULATOR: A BRIDGE TO RELIABLE SIMULATIONS

Randall J. McDermott
National Institute of Standards and Technology
Gaithersburg, Maryland, USA
e-mail: randall.mcdermott@nist.gov

ABSTRACT

In this paper, we examine the emerging field of *quality assessment* for large-eddy simulation of fire dynamics. The importance of model convergence is discussed and the differences between validation and quality assessment are highlighted. Briefly, validation compares a model to experimental data, whereas quality assessment fills the void between experiments and practical applications. Two quality metrics are discussed: a measure of turbulence resolution and a normalized wavelet error measure. The metrics are monitored in a simulation of the Sandia 1 m methane pool fire and target metric values are inferred based on the results of a grid resolution study.

INTRODUCTION

The emerging field of *quality assessment* for computational models is not a panacea. But it is close.

Quality assessment (QA) represents a shift in thinking away from the idea that model validation is the end goal. Validation is certainly a necessary means to an end. But it requires experiment, and if an experiment exists, it is unlikely we need a model to begin with. QA is about filling in the space between validation points. It is about evaluating the quality of a model result *without* the luxury of experimental data.

The intent of this paper is not to debate what we mean by validation or when we may consider a model to be validated. This has been done by Oberkampf [1] and McGrattan [2]. In this paper, we discuss how to assess the quality of numerical solutions in the absence of corroborating data, where a model is most useful for prediction.

QA for large-eddy simulation (LES) unofficially began in 1996 with the seminal work of Ghosal [3], who demonstrated the resolution requirements for various numerical schemes in the context of *explicit filtering* (see [4, 5] for a review of filtering in LES). In short, Ghosal showed that with a second-order scheme a filter-width-to-grid-spacing ratio of $\Delta/\delta x \geq 8$ is required in order for numerical error to be small ($<10\%$) compared to the magnitude of the terms in the physical model (later we will discuss in more detail the roles of both Δ and δx in generating numerical solutions to the partial differential equations which form the basis of LES). Thus, explicit filtering requires the model to run 4096 times slower (8^4, eight levels of refinement in each of three spatial dimensions and one temporal dimension) for the same spatial resolution—a demoralizing prospect for engineering codes.

Fortunately, recent experience has shown that the practice of *implicit filtering* ($\Delta/\delta x$=1) is permissible for modeling statistically stationary or mildly statistically transient flows (prevalent in engineering applications) provided the numerical methods (a) conserve kinetic energy [6, 7] and (b) are convergent (more on this later). The Fire Dynamics Simulator (FDS), which is the subject of the present paper, is an implicitly filtered, second-order accurate LES code.

The QA methods presented in this paper are primarily aimed at engineering applications. In what follows, we narrow our scope to focus on mesh quality for gas phase phenomena. The reader should note, however, that sufficient mesh quality by no means guarantees a sufficiently accurate model result. It is merely one component of the fire model, but it is the only one where QA methods exist. We hope the ideas presented here will spark QA research in the more problematic areas of fire modeling, such as the burning solid phase material.

The important length scale for resolution of prescribed buoyant pool fires is the minimum between the fire height and the characteristic diameter of the fire [8],

$$D^* = \left(\frac{\dot{Q}}{\rho_\infty c_p T_\infty \sqrt{g}} \right)^{2/5}. \qquad (1)$$

Here, $\dot{Q}$ is the total heat release of the fire, ρ_∞ is the ambient density, c_p is the ambient specific heat, T_∞ the ambient temperature, and g is gravity. Current guidance in FDS is to keep $D^*/\delta x = O(10)$ (results in the FDS Validation Guide [9] generally range from 5 to

20). This has been the implied QA metric for LES models of prescribed fires. The shortcoming of this approach is that it cannot be extended to modeling flame *spread* and it is of little use for optimizing mesh density in adaptive mesh refinement (AMR), a technique which holds promise for drastically improving fidelity and speed of fire simulations.

The modern view on LES QA is summarized in the proceedings of the Workshop on Quality and Reliability of Large-Eddy Simulations [10]. The usual strategy is to examine run-time mesh quality metrics, and to use this information to guide refinement (or coarsening) of the grid as necessary. In this paper, we present a metric from the literature based on modeling the fraction of unresolved kinetic energy (the Pope criterion [11]). We also present a new error metric based on a simple Haar wavelet transform. Both metrics can be output by FDS.

The remainder of the paper is organized as follows: Before examining the QA metrics in detail, we survey our challenge by trying to gain an appreciation for the volume of application space not covered by experimental validation and therefore squarely under the responsibility of quality assessment. Next, we comment on an important prerequisite for the success of the QA process, namely, that the LES code must be *convergent*. After presentation of the metrics, we provide an example of how they may be applied.

APPLICATION SPACE

We get asked all the time, "What are the limitations of FDS?" Some limitations are obvious enough: the code is not designed for compressible flows; it cannot handle non-Newtonian fluids, liquids, or (at present) curvilinear and moving goemetries. Some limitations are not so obvious. For example, today flame spread is still very much a research area. The limitations of pyrolysis models (including the availability of material properties) in addition to the chaotic nature of flame propagation make this problem extremely difficult. As a result, some FDS simulations of flame spread may be accurate while others may be way off mark. So how is a user to know whether to trust the answer?

The usual response to this question is to look at the Validation Guide [9]. If the code (in this case FDS) has been "validated" for the application, then the answer must be trustworthy. Right?

There are two issues to address here. The first is that the setup and mesh resolution chosen by the user are important to the quality of the results. We will discuss some aspects of this in the next section. But actually, the more vexing issue is that the probability of the user finding the exact case they are looking for in the Validation Guide is nil. More generally, if experimental data (or a correlation) exists with which to validate a simulation, from an engineering perspective, the model may not be especially useful. The cases we are usually interested in (the ones engineering firms get paid to analyze) are the ones without validation data (if we are designing a new skyscraper, we are probably not going to burn it down to see if our fire safety design was accurate). Are *all* these applications outside the limitations of the model? Hopefully not.

This raises a serious and legitimate question: How far can we stray from the experimental data? Usually, developers (of just about any model) make the claim that the model has been validated for some *class* of applications (plumes, for example). This is clean and tidy when the problem class can be well defined in terms of one or two dimensionless parameters (maybe a Reynolds number or a Froude number). Real life is not so easy. The parameter space will have many, many dimensions without nice clean scaling laws.

To help visualize the predicament, in Figure 1 we present a *hypothetical* two-dimensional application space (real application space is an n-dimensional hypercube). The interior of each black outlined region (circle or rectangle) represents a problem class and the blue dots represent individual validation experiments within the class. The red box represents the theoretical applicability of the model. There are two points to make about this space. The first is that the volume of space where the model is theoretically applicable may be large compared to the volume of the validation space. The second point is that the landscape of the space between validation classes may not be smooth. So, interpolation between validation classes or combining model results from neighboring classes may not be valid without additional analysis (and faith in the physics of the model, which effectively becomes a sophisticated interpolant between validated regions of the space). An example of the type of argument often made is to say that a model has been validated for plumes and that it has been validated for duct flows and then to claim the model is therefore valid for the problem of a plume in a compartment ventilated by a duct (for which specific experimental data may not exist). This would be a case within the red square (theoretical applicability of the model) but where quality assessment of the result would be critical.

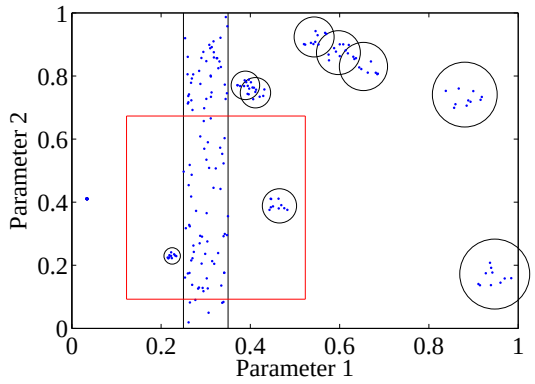

Figure 1: A *hypothetical* two-dimensional application space. Blue dots represent validation experiments. The black outlined regions represent classes of flows. The red square represents the region of theoretical applicability of the model. The empty space (the anti-library [12]) is infinite in volume.

LES TO DNS CONVERGENCE

The notion of achieving "sufficient resolution" presupposes that higher resolution yields better answers. While this seems like an obvious requirement to build into a computational fluid dynamics (CFD) model, achieving this ideal in practice is not so simple. As shown below, if we are not careful, we may run into trouble with physical models or numerical methods or both. (The reader not interested in devilish mathematical details may safely skip the rest of this section.)

First, we need to understand the difference between direct numerical simulation (DNS) and large-eddy simulation (LES). For simplicity, we will only examine the species transport equation:

$$\frac{\partial \rho Y_\alpha}{\partial t} + \frac{\partial (\rho Y_\alpha u_i)}{\partial x_i} = \frac{\partial}{\partial x_i}\left(\rho D_\alpha \frac{\partial Y_\alpha}{\partial x_i}\right) + \dot{m}'''_\alpha \,. \qquad (2)$$

Here, ρ is the density, Y_α is the mass fraction of species α, u_i is the ith component of velocity, D_α is the mixture-averaged diffusivity of α, and $\dot{m}'''_\alpha$ is the chemical source term. Let us imagine that (2) is an adequate representation of the physical system (Fick's law with mixture-averaged diffusivity is appropriate) such that an *accurate* numerical solution may be considered a DNS (if a simulation is truly a DNS, it may be considered a substitute for experiment—any user turning to "DNS" mode in FDS should apply this standard of quality).

The LES equations are derived by applying a low-pass filter, of characteristic width Δ, the filter width, to the DNS equations. For our purposes, filtered fields may be thought of as cell means, which we denote with an overbar, and when the filter is applied to (2) we obtain

$$\frac{\partial \overline{\rho Y_\alpha}}{\partial t} + \frac{\partial (\overline{\rho Y_\alpha u_i})}{\partial x_i} = \frac{\partial}{\partial x_i}\left(\overline{\rho D_\alpha \frac{\partial Y_\alpha}{\partial x_i}}\right) + \overline{\dot{m}'''_\alpha} \,. \qquad (3)$$

Simple enough, we just put bars over everything. Trouble is, we have no way of computing the stuff under the bars to advance (3) in time. We must decompose the terms, and this leads to closure problems.

The first step is to define a mass-weighted average (Favre-average) such that for any quantity $\overline{\rho\phi} = \bar{\rho}\tilde{\phi}$. Applying this decomposition to (3) and making a subtle approximation to the diffusive term leads to

$$\frac{\partial \bar{\rho}\tilde{Y}_\alpha}{\partial t} + \frac{\partial (\bar{\rho}\widetilde{Y_\alpha u_i})}{\partial x_i} = \frac{\partial}{\partial x_i}\left(\bar{\rho}\tilde{D}_\alpha \frac{\partial \tilde{Y}_\alpha}{\partial x_i}\right) + \overline{\dot{m}'''_\alpha} \,. \qquad (4)$$

Note that we still have no way to compute the correlation $\widetilde{Y_\alpha u_i}$ on the grid. We cannot simply substitute $\tilde{Y}_\alpha \tilde{u}_i$ (this is the old problem of "the mean of the square does not equal the square of the mean"). Instead, we define the *subgrid* flux,

$$J^{sgs}_{\alpha,i} \equiv \bar{\rho}(\widetilde{Y_\alpha u_i} - \tilde{Y}_\alpha \tilde{u}_i) \,, \qquad (5)$$

and substitute this flux into (4) to obtain

$$\frac{\partial \bar{\rho}\tilde{Y}_\alpha}{\partial t} + \frac{\partial (\bar{\rho}\tilde{Y}_\alpha \tilde{u}_i)}{\partial x_i} = \frac{\partial}{\partial x_i}\left(\bar{\rho}\tilde{D}_\alpha \frac{\partial \tilde{Y}_\alpha}{\partial x_i}\right) - \frac{\partial J^{sgs}_{\alpha,i}}{\partial x_i} + \overline{\dot{m}'''_\alpha} \,. \qquad (6)$$

This is the LES species transport equation. It remains that we find suitable models for $J^{sgs}_{\alpha,i}$ and $\overline{\dot{m}'''_\alpha}$, and, to achieve LES to DNS convergence, that we prove $J^{sgs}_{\alpha,i} \to 0$ and $\overline{\dot{m}'''_\alpha} \to \dot{m}'''_\alpha$ as $\Delta \to \eta$ (the smallest length scales of the flow).

Convergence of physical models

In FDS, the subgrid flux is modeled with an eddy diffusivity taken from the turbulent viscosity and a constant turbulent Schmidt number,

$$J^{sgs}_{\alpha,i} = -\frac{\mu_t}{\mathrm{Sc}_t}\frac{\partial \tilde{Y}_\alpha}{\partial x_i} \,. \qquad (7)$$

For convergence, we require $\mu_t \to 0$ as $\Delta \to \eta$. For the constant coefficient Smagorinsky model the turbulent viscosity is given by

$$\mu_t = \bar{\rho}(C_s\Delta)^2|\tilde{S}| \,, \qquad (8)$$

where C_s is the Smagorinsky constant, $|S|$ is the magnitude of the strain rate tensor with components $S_{ij} =$

$\frac{1}{2}(\partial_j u_i + \partial_i u_j)$. Note that both $\bar{\rho} \to \rho$ and $|\tilde{S}| \to |S|$ as $\Delta \to \eta$ at a second-order rate, which suffices. But now consider the evaluation of μ_t at $\Delta = \eta$. First, note that the kinetic energy dissipation rate is given by $\varepsilon = 2\nu S_{ij} S_{ij} = \nu |S|^2$, where ν is the kinematic viscosity of the fluid. Also, from Kolmogorov (see [5]) we have $\eta = (\nu^3/\varepsilon)^{1/4}$. Using these relationships in (8) we find the turbulent viscosity becomes

$$\begin{aligned} \frac{\mu_t}{\rho} &= (C_s \eta)^2 |S| \\ &= (C_s \eta)^2 \left(\frac{\varepsilon}{\nu}\right)^{1/2} \\ &= C_s^2 \left(\frac{\nu^3}{\varepsilon}\right)^{1/2} \left(\frac{\varepsilon}{\nu}\right)^{1/2} \\ &= C_s^2 \frac{\nu^{3/2}}{\nu^{1/2}} = C_s^2 \nu = C_s^2 \frac{\mu}{\rho}. \end{aligned} \tag{9}$$

As we can see, the turbulent viscosity never goes away, we are left with a guaranteed 4% error ($C_s^2 \nu \approx 0.04\,\nu$).

This is one reason why the dynamic procedure [13, 14] for evaluating the model constant is preferred since the dynamically computed Smagorinsky coefficient C_s vanishes as $\Delta \to \eta$. This issue is more important than it seems at first glance. Problems with the constant coefficient model actually emerge with $\Delta \gg \eta$. Real turbulent flows are intermittent (local pockets of laminar flow) with large bursts of forward energy transfer (large scale motions cascading to small scales) and high levels of "backscatter" (small scales generating large scale motions). Backscatter is extremely challenging to get right, but at a minimum we would like our models to turn themselves off rather than transfer energy in the wrong direction [22].

Practical Considerations

As another example of possible convergence issues, consider the radiation source term. FDS operates in either "LES mode" (default) or "DNS mode" and this simple switch also switches the model for radiant emission. In LES mode, the emission intensity is set to the maximum of $\kappa\sigma T^4/\pi$ and $\chi_r \dot{q}'''/4\pi$, where χ_r is a constant radiant fraction, $\dot{q}'''$ is the heat release per unit volume, T is temperature, κ is the absorption coefficient, and σ is the Stefan-Boltzmann constant. In most cases, the T^4 law will dominate at fine grid resolution, but this is not guaranteed (depends on χ_r). Still, this example illustrates a case where the solution is so practical (simple, robust) that we are willing to live with the potential convergence problem.

Convergence of numerical methods

Numerical methods to solve (6) involve approximations to mass fluxes and spatial derivatives, and techniques for integrating the solution forward in time. To illustrate how the numerics may lead to convergence problems, consider the mass fluxes in the advective term of the species transport equation. In 1D, for a given cell i, the advective term is approximated by

$$\frac{\partial(\bar{\rho}\tilde{Y}_\alpha \tilde{u})}{\partial x} \approx \frac{(\bar{\rho}\tilde{Y}_\alpha \tilde{u})_{i+1/2} - (\bar{\rho}\tilde{Y}_\alpha \tilde{u})_{i-1/2}}{\delta x} \tag{10}$$

In the staggered storage arrangement used by FDS the velocity component lives at the cell face, denoted $i+1/2$, so these values need no interpolation. The density and mass fractions, however, are stored at the cell center and must be interpolated to the cell face to form the flux. This simple task is of critical importance to the accuracy, stability, and convergence of any CFD code.

The two most common methods of handling the interpolation are central differencing and upwinding (Godunov's method, see [15]). Central differencing is second-order for *smooth* solutions and Godunov's method is first-order. When central differencing encounters any data variations which are not smooth, it admits spurious (nonphysical) oscillations known as Gibbs oscillations. The error generated by the central scheme is called *numerical dispersion*. The error generated by the first-order Godunov scheme is called *numerical diffusion*. The character of the two types of error are qualitatively different. The diffusion error ultimately convergences to zero, albeit at a slow rate. The dispersion error does not converge and may lead to instability. What often happens in a CFD code is that the dispersion error is kept in check by physical diffusion. But in this case one never knows what real damage is being done to the integrity of the solution. For LES, we have learned it is important to check the integrity of the solution in the abscence of physical diffusion. If the character of the advection solution is correct, physical diffusion is more accurately represented.

To show the qualitative difference one can expect with different transport schemes (that is, different ways of interpolating the density and mass fractions to the cell face), below we present two solutions to the problem of linear advection of square waves in 2D. The domain is a unit square with 80×80 grid resolution. The Courant number (time-step criterion) is 0.25. The initial condition is shown in Figure 2. The color contours represent a species mass fraction. The block in the

lower left (red) has a value of one and the block in the upper right (green) has a mass fraction of one half. The diffusivity is set to zero. The horizontal and vertical components of velocity are held constant at $u = 1$ and $w = 1$. In the true solution to this problem, the square blocks simply advects diagonally to the upper right and, with a periodic domain, after one flow through time arrive again exactly at the initial state (Figure 2 is therefore both the initial state and final state of the exact solution).

In Figure 3, we show the resulting numerical solution at one flow through time for a convergent transport scheme, the CHARM flux limiter [16]. This scheme is second-order for smooth solutions (unlike Godunov) and convergent for both square (not smooth) and sinusoidal waves. In Figure 4, we show the results from a bounded central scheme. Bounded schemes use central differencing except in locations where the scalar value goes "out of bounds", such as a mass fraction going outside the range [0,1]. The dispersion error of the central scheme tries to create boundedness violations. These violations are contained in the first block (lower left), though the integrity of the solution is clearly degraded. For the second block, the dispersion generates a "checker board" pattern. Such behavior can be problematic for reacting flows if fictitious new stoichiometric surfaces are created. And, to the point about convergence, if the grid is refined, the dispersion error persists.

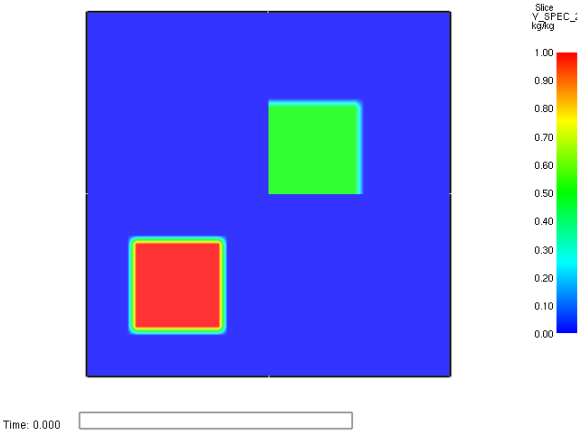

Figure 2: Initial condition and exact solution final state.

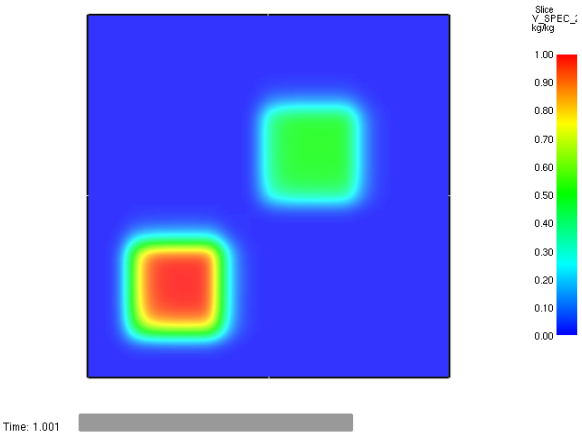

Figure 3: Convergent transport scheme (CHARM flux limiter).

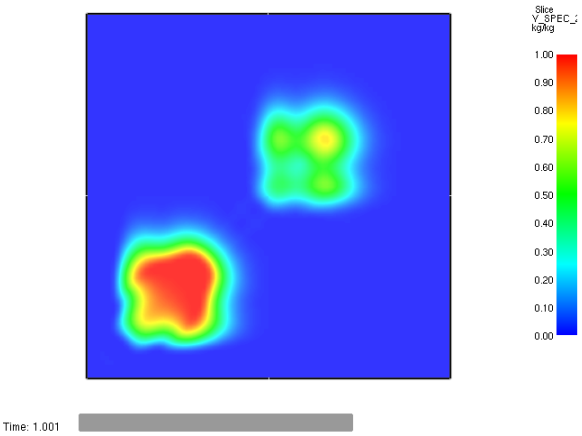

Figure 4: Non-convergent scheme (bounded central).

TURBULENCE RESOLUTION

In FDS, the user may output a scalar quantity which we refer to as the *measure of turbulence resolution* (MTR), defined locally as

$$\mathrm{MTR}(\mathbf{x},t) = \frac{k_{sgs}}{k_{res}+k_{sgs}} \tag{11}$$

where the *resolved* (*res*) and *subgrid-scale* (*sgs*) kinetic energies are given by

$$k_{res} = \tfrac{1}{2}\tilde{u}_i\tilde{u}_i \tag{12}$$

$$k_{sgs} = \tfrac{1}{2}(\tilde{u}_i - \hat{\tilde{u}}_i)(\tilde{u}_i - \hat{\tilde{u}}_i) \tag{13}$$

Here, $\tilde{u}_i$ is the resolved LES velocity and $\hat{\tilde{u}}_i$ is test filtered at a scale 2Δ where Δ is the LES filter width (recall, in FDS, $\Delta = \delta x$). The model for the subgrid fluctuations is taken from scale similarity [17].The basic idea is to provide the user with an easily accessible

approximation to the Pope Criterion [11]. In Smokeview (FDS visualization software), the user may readily time average MTR in a specified plane. The time average of MTR is a reasonable estimate of the Pope Criterion. The measure falls within the range [0,1], with 0 indicating perfect resolution (like the best high-definition television picture possible) and 1 indicating no resolution (as if the television screen had only one pixel, one color). The concept is illustrated in Figures 5 and 6. Notice that in Figure 5 the difference between the grid signal and the test signal is very small. In Figure 6, the grid signal is highly turbulent and the corresponding test signal is much smoother. We infer then that the flow is under-resolved.

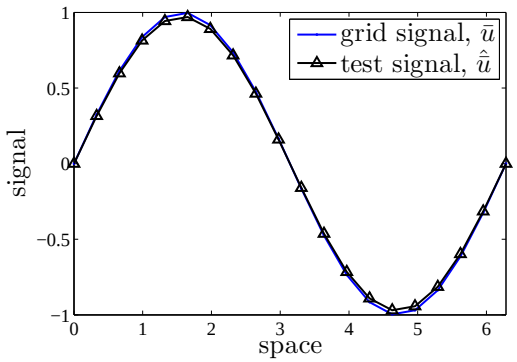

Figure 5: Resolved signal, MTR is small.

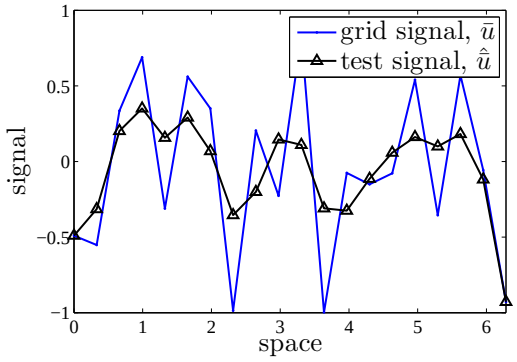

Figure 6: Unresolved signal, MTR close to unity.

For the canonical case of isotropic turbulence Pope actually defines LES such that $\langle \text{MTR} \rangle < 0.2$. That is, LES requires resolution of 80% of the kinetic energy in the flow field (for sufficiently high Reynolds number, this puts the grid resolution length scale within the inertial subrange—the range of scales which exhibit isotropy and universality, unaffected by the geometry of the flow problem). The question remains as to whether this critical value is sufficient or necessary for a given engineering problem.

WAVELET ERROR MEASURE

We begin by providing background on the simple Haar wavelet [18]. For a thorough and more sophisticated review of wavelet methods, the reader is referred to Schneider and Vasilyev [19].

Suppose the scalar function $f(r)$ is sampled at discrete points r_j, separated by a distance h, giving values s_j. Defining the *unit step function* over the interval $[r_1, r_2]$ by

$$\varphi_{[r_1,r_2]} = \begin{cases} 1 & \text{if} \quad r_1 \le r < r_2 \\ 0 & \text{otherwise} \end{cases} \tag{14}$$

the simplest possible reconstruction of the signal is the step function approximation

$$f(r) \approx \sum_j s_j \varphi_{[r_j, r_j+h]}(r) \tag{15}$$

By "viewing" the signal at a coarser resolution, say $2h$, an identical reconstruction of the function f over the interval $[r_j, r_j+2h]$ may be obtained from

$$\begin{aligned} f_{[r_j,r_j+2h]}(r) &= \underbrace{\tfrac{s_j+s_{j+1}}{2}}_{a} \varphi_{[r_j,r_j+2h]}(r) \\ &+ \underbrace{\tfrac{s_j-s_{j+1}}{2}}_{c} \psi_{[r_j,r_j+2h]}(r) \end{aligned} \tag{16}$$

where a is as the *average* coefficient and c is as the *wavelet* coefficient. The Haar *mother wavelet* (Figure 7) is identified as

$$\psi_{[r_1,r_2]}(r) = \begin{cases} 1 & \text{if} \quad r_1 \le r < \frac{1}{2}(r_1+r_2) \\ -1 & \text{if} \quad \frac{1}{2}(r_1+r_2) \le r < r_2 \end{cases} \tag{17}$$

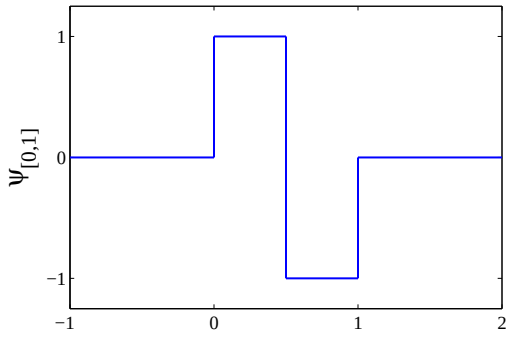

Figure 7: Haar mother wavelet on the interval [0,1].

The decomposition of the signal shown in (16) may be repeated at ever coarser resolutions. The result is a *wavelet transform*. The procedure is entirely analogous to the Fourier transform, but with compact support (only local grid data is required). If we look at a 1D signal with 2^m points, the repeated application of (16) results in an $m \times m$ matrix of averages $\mathbf{a}$ with components a_{ij} and an $m \times m$ wavelet coefficient matrix $\mathbf{c}$ with components c_{ij}. Each row i of $\mathbf{a}$ may be reconstructed from the $i+1$ row of $\mathbf{a}$ and $\mathbf{c}$. Because of this and because small values of the wavelet coefficient matrix may be discarded, dramatic compression of the signal may be obtained.

Here we are interested in using the wavelet analysis to say something about the local level of error due to grid resolution. Very simply, we ask what can be discerned from a sample of four data points along a line. Roughly speaking we might expect to see one of the four scenarios depicted in Figures 8-11. After each plot we also show the results of a Haar wavelet transform for that signal. Note that with four points $m = 2$ ($4 = 2^2$) and the average and coefficient matrices are 2×2.

Looking at Figures 8 and 9, first we have a straight line and below this a step function. Intuitively, we expect zero error for the line (over-resolved) and large error for the step function (under-resolved). The following wavelet error measure (WEM) achieves this goal:

$$\mathrm{WEM}(\mathbf{x},t) = \max_{x,y,z}(|c_{11} + c_{12} - c_{21}|) \qquad (18)$$

Equation (18) represents the main contribution of this paper. Note that the wavelet coefficients c_{ij} are based on the transform of a normalized signal. That is, the four data points being transformed are first rescaled to have min 0 and max 1. The metric compares the wavelet coefficients at two different resolutions. Based on this measure, a linear signal (Figure 8), which is clearly over-resolved, has WEM=0, the step function (Figure 9) has WEM=1/2, the extrema (Figure 10) has WEM=0 (a quadratic curve is perfectly resolved by a second-order scheme), and the noisy signal (Figure 11) endemic of Gibbs oscillation (numerical dispersion error) gives the worst case with WEM=1.

In practice the transform is performed in all coordinate directions and the max value is reported. The scalar value may be output to Smokeview at the desired time interval and averaged in time.

EXAMPLE

The Sandia 1 m methane pool fire, Test 17 (high flow rate) [20, 21], is simulated using three grid resolutions: 6 cm, 3 cm, and 1.5 cm. These grid resolutions correspond to $D^*/\delta x$ of 25, 50, and 100, respectively. Such high resolution is atypical of engineering calculations using FDS. But in this validation example, we are comparing the model results against detailed velocity measurements within one diameter of the base of the pool. Previous works [1, 22] have shown similar resolution is required to capture the details of the flow in this region.

The computational setup is outlined in the FDS Validation Guide [9]. To provide the reader with a qualitative feel for the results, Figure 12 shows a snapshot of temperature contours from the 1.5 cm simulation. The calculations are run in parallel on 16 processors. Data for vertical velocity and radial velocity are recorded at three levels downstream from the base of the plume, $z = [0.3, 0.5, 0.9]$ m. Results for the mean profiles are given in Figure 13. The means are taken between $t = 10$ and $t = 20$ s in the simulation.

As can be seen from Figure 13, the 3 cm and 1.5 cm results seem to be converging. There are, however, still inaccuracies near the outer edge of the pool. This may be the result of insufficient grid resolution or inaccuracies in the boundary conditions. Or, even if the code is convergent, these inaccuracies may be directly linked to inaccuracies in specific model components, such as a simplified reaction model. If the code has converged, improving these results falls under the purview of validation. But it is possible that we have fortuitously reached a plateau in the statistics as a function of grid resolution [11]. The model may have more than one plateau before true convergence is achieved.

Here we are interested in saying something about the quality of the gas phase grid resolution. Arguably, the 3 cm case is sufficiently resolved for our purposes—the results are improved over the coarse simulation and the refined simulation shows no appreciable change. By examining the quality metrics defined earlier in this paper, we can now draw conclusions about metric targets for practical problems. Figures 14-19 show split contour plots of (left) the measure of turbulence resolution (MTR) and (right) wavelet error measure (WEM). The metrics are averaged in time over the last 10 s of the simulation. The turbuence color contours are split at the theoretical value of MTR=0.2 (80% of the turbulent kinetic energy is resolved) and the WEM contours are split at 0.3 (this choice will be discussed later).

First, note that an output anomaly is present at mesh

boundaries. This is particularly noticeable in the MTR cases where MTR is close to unity near the mesh boundaries. This issue arises because we do not want to consume computational time exchanging information via message passing (parallel computing) during the output phase of the run. Better handling of the metric boundary values is work in progress.

Looking more closely at the turbulence metric, we can see from Figure 14 ($\delta x = 6$ cm) that the bulk of the domain is above 0.2. As the resolution is increased, the metric decreases and at 3 cm—which we have deemed sufficient resolution—MTR is generally below 0.2. Notice that the shear layer near the edge of the pool shows the highest legitimate values of the metric (that is, aside from the mesh boundary anomaly). This metric, therefore, appears to behave precisely as we would like—there seems to exist a critical value where reasonably accurate simulation results can be expected (we take "reasonably accurate" to mean the simulation results fall within experimental uncertainty).

Let us now examine Figures 17-19, which show the normalized wavelet error for the fuel (methane) mass fraction field. Unlike the turbulence metric, with WEM we do not (as of yet) have a good theoretical target. By examining the 3 cm results we can infer that WEM=0.3 is adequate. By setting this as the color contour split we notice something interesting: even the 1.5 cm case under-resolves the fuel mass fraction field in the shear layer near the base of the pool. This raises the question of whether the 1.5 cm simulation is really sufficiently resolved in this region, which may be the cause of the inaccuracy in the mean velocity at the outer edge. This is a perfect example to illustrate why adaptive mesh refinement (AMR) is useful. The volume of the shear layer region is very small, yet requires very high resolution to get right.

CONCLUSIONS

In this paper, we have presented two mesh quality metrics: a measure of turbulence resolution and a wavelet error measure. Each of these may be output to an FDS slice file or device for monitoring. Using the example of the Sandia 1 m methane pool fire, we confirmed that the theoretical value of MTR = 0.2 works well in practice for identifying adequate mesh resolution for capturing velocity statistics in the near field of the pool fire. We also found that keeping the species concentration wavelet error (WEM) below 0.3 is an added constraint. It is important to point out that this *does not* imply $D^*/\delta x = 50$ (recall, this corresponds to the $\delta x = 3$ cm case) is required to achieve adequate results for all engineering problems. It depends on the question being asked of the model. In the example shown here, we are trying to capture inflections in the mean velocity contours at the base of a large-scale pool fire. As stated earlier, most of the cases in the FDS Validation Guide [9] do not require such high resolution.

We should point out that species mass fractions are not the only values which we can examine with the wavelet metric. Any quantity valid for slice file output in FDS may be examined for wavelet error. In the future we plan to look at quantities such as temperature and heat release rate to see if these metrics are better indicators of mesh quality.

ACKNOWLEDGMENTS

I am indebted to Sheldon Tieszen for generously providing his data on the Sandia plume experiments. I would also like to thank Jason Floyd, Kevin McGrattan, Taylor Myers, Michael Spearpoint, and Jason Averill for their critiques and insightful discussions.

REFERENCES

[1] W. L Oberkampf and M. F. Barone. Measures of agreement between computation and exmperiment: validation metrics. *J. Comp. Phys.*, 217:5–36, 2006. 1, 7

[2] K. McGrattan and B. Toman. Quantifying the predictive uncertainty of complex numerical models. *Metrologia*, 48:173–180, 2011. 1

[3] S. Ghosal. An analysis of numerical errors in large-eddy simulation of turbulence. *J. Comp. Phys.*, 125:187–206, 1996. 1

[4] T. S. Lund. On the use of discrete filters for large eddy simulation. In *Stanford Center for Turbulence Research Annual Research Briefs*, 1997. 1

[5] Stephen B. Pope. *Turbulent Flows*. Cambridge, 2000. 1, 4

[6] R. Mittal and P. Moin. Suitability of upwind-biased finite difference schemes for large-eddy simulation of turbulent flows. *AIAA Journal*, 35(8):1415–1417, 1997. 1

[7] Y. Morinishi, T. S. Lund, O. V. Vasilyev, and P. Moin. Fully conservative high order finite difference schemes for incompressible flow. *J. Comp. Phys.*, 143:90–124, 1998. 1

[8] G. Heskestad. *SFPE Handbook of Fire Protection Engineering (4th ed.)*, chapter Fire Plumes, Flame Height and Air Entrainment. National Fire Protection Association, 2008. 1

[9] K. McGrattan, S. Hostikka, J. Floyd, and R. McDermott. Fire dynamics simulator (version5), technical reference guide, volume 3: Validation. NIST Special Publication 1018-5, National Institute of Standards and Technology, Gaithersburg, Maryland, September 2010. 1, 2, 7, 8

[10] J. Meyers, B. Geurts, and P. Sagaut, editors. *Quality and Reliability of Large-Eddy Simulations*. Springer, 2008. 2

[11] S. B. Pope. Ten questions concerning the large-eddy simulation of turbulent flows. *New J. Phys.*, 6:1–24, 2004. 2, 6, 7

[12] Nassim N. Taleb. *The Black Swan: The Impact of the Highly Improbable*. Random House Trade Paperback, 2010. 3

[13] M. Germano, U. Piomelli, P. Moin, and W. Cabot. A dynamic subgrid-scale eddy viscosity model. *Phys. Fluids A*, 3(7):1760–1765, 1991. 4

[14] P. Moin, K. Squires, W. Cabot, and S. Lee. A dynamic subgrid-scale model for compressible turbulence and scalar transport. *Phys. Fluids A*, 3(11):2746–2757, 1991. 4

[15] E. F. Toro. *Riemann Solvers and Numerical Methods for Fluid Dynamics: A Practical Introduction*. Springer, 1999. 4

[16] G. Zhou. *Numerical simulations of physical discontinuities in single and multi-fluid flows for arbitrary Mach numbers*. PhD thesis, Chalmers Univ. of Tech., Goteborg, Sweden, 1995. 5

[17] J. Bardina, J. H. Ferziger, and W. C. Reynolds. Improved subgrid scale models for large-eddy simulation. *AIAA Paper 80-1357*, 1980. 5

[18] Yves Nievergelt. *Wavelets Made Easy*. Birkhäuser, 2001. 6

[19] K. Schneider and O. Vasilyev. Wavelet methods in computational fluid dynamics. *Annu. Rev. Fluid Mech.*, 42:473–503, 2010. 6

[20] S. R. Tieszen, T. J. O'Hern, R. W. Schefer, E. J. Weckman, and T. K. Blanchat. Experimental study of the flow field in and around a one meter diameter methane fire. *Combust. Flame*, 129:378–391, 2002. 7

[21] S. R. Tieszen, T. J. O'Hern, E. J. Weckman, and R. W. Schefer. Experimental study of the effect of fuel mass flux on a 1-m-diameter methane fire and comparison with a hydrogen fire. *Combust. Flame*, 139:126–141, 2004. 7

[22] P. E. DesJardin, T. J. O'Hern, and S. R. Tieszen. Large eddy simulation and experimental measurements of the near-field of a large turbulent helium plume. *Phys. Fluids*, 16(6):1866–1883, 2004. 4, 7

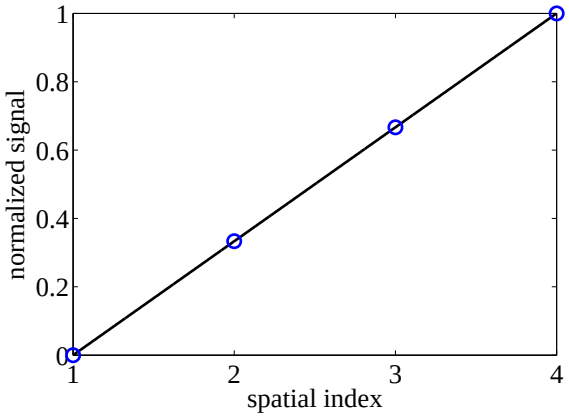

$$\mathbf{a} = \begin{bmatrix} 0.17 & 0.83 \\ 0.5 & 0 \end{bmatrix}; \quad \mathbf{c} = \begin{bmatrix} -0.17 & -0.17 \\ -0.33 & 0 \end{bmatrix}$$

Figure 8: Straight line. Over-resolved, WEM=0.

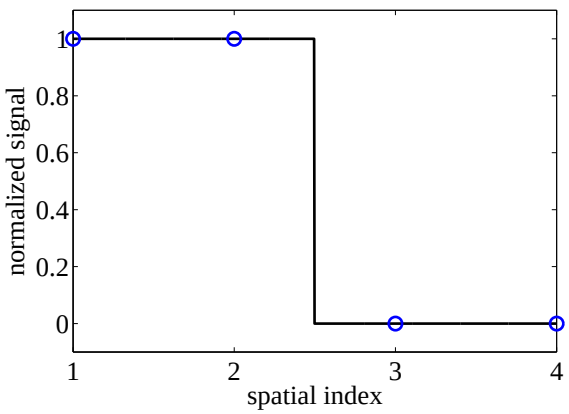

$$\mathbf{a} = \begin{bmatrix} 1 & 0 \\ 0.5 & 0 \end{bmatrix}; \quad \mathbf{c} = \begin{bmatrix} 0 & 0 \\ 0.5 & 0 \end{bmatrix}$$

Figure 9: Step function. Under-resolved, WEM=1/2.

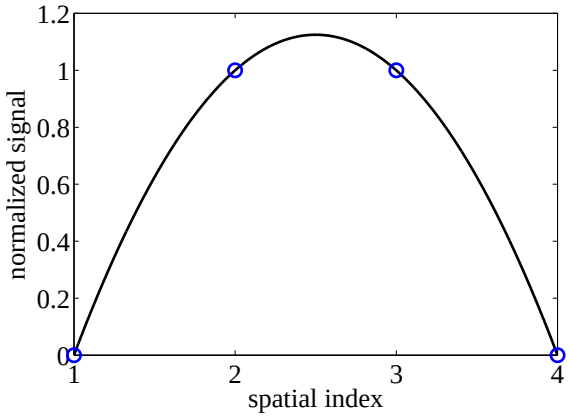

$$\mathbf{a} = \begin{bmatrix} 0.5 & 0.5 \\ 0.5 & 0 \end{bmatrix}; \quad \mathbf{c} = \begin{bmatrix} -0.5 & 0.5 \\ 0 & 0 \end{bmatrix}$$

Figure 10: Quadratic extrema perfectly resolved by a second-order centered scheme, WEM=0.

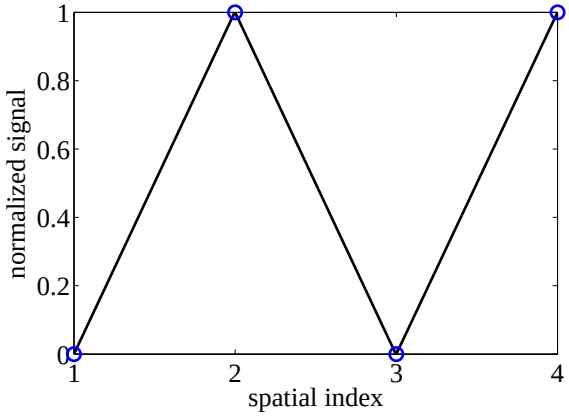

$$\mathbf{a} = \begin{bmatrix} 0.5 & 0.5 \\ 0.5 & 0 \end{bmatrix}; \quad \mathbf{c} = \begin{bmatrix} -0.5 & -0.5 \\ 0 & 0 \end{bmatrix}$$

Figure 11: Noisy signal endemic of Gibbs oscillation, WEM=1.

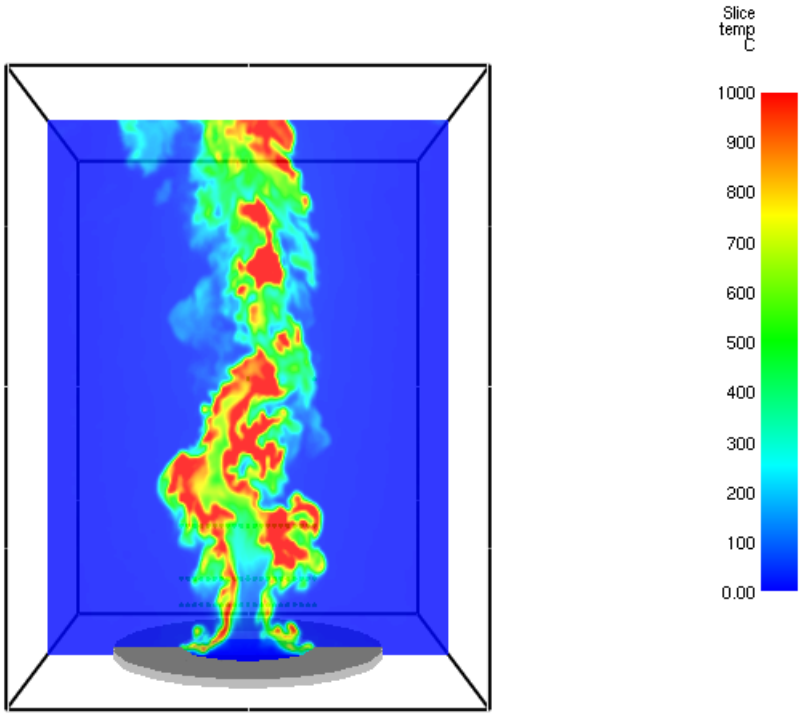

Figure 12: A snapshot of FDS results at 1.5 cm resolution for the Sandia 1 m methane pool fire (Test 17 – high flow rate) showing instantaneous contours of temperature.

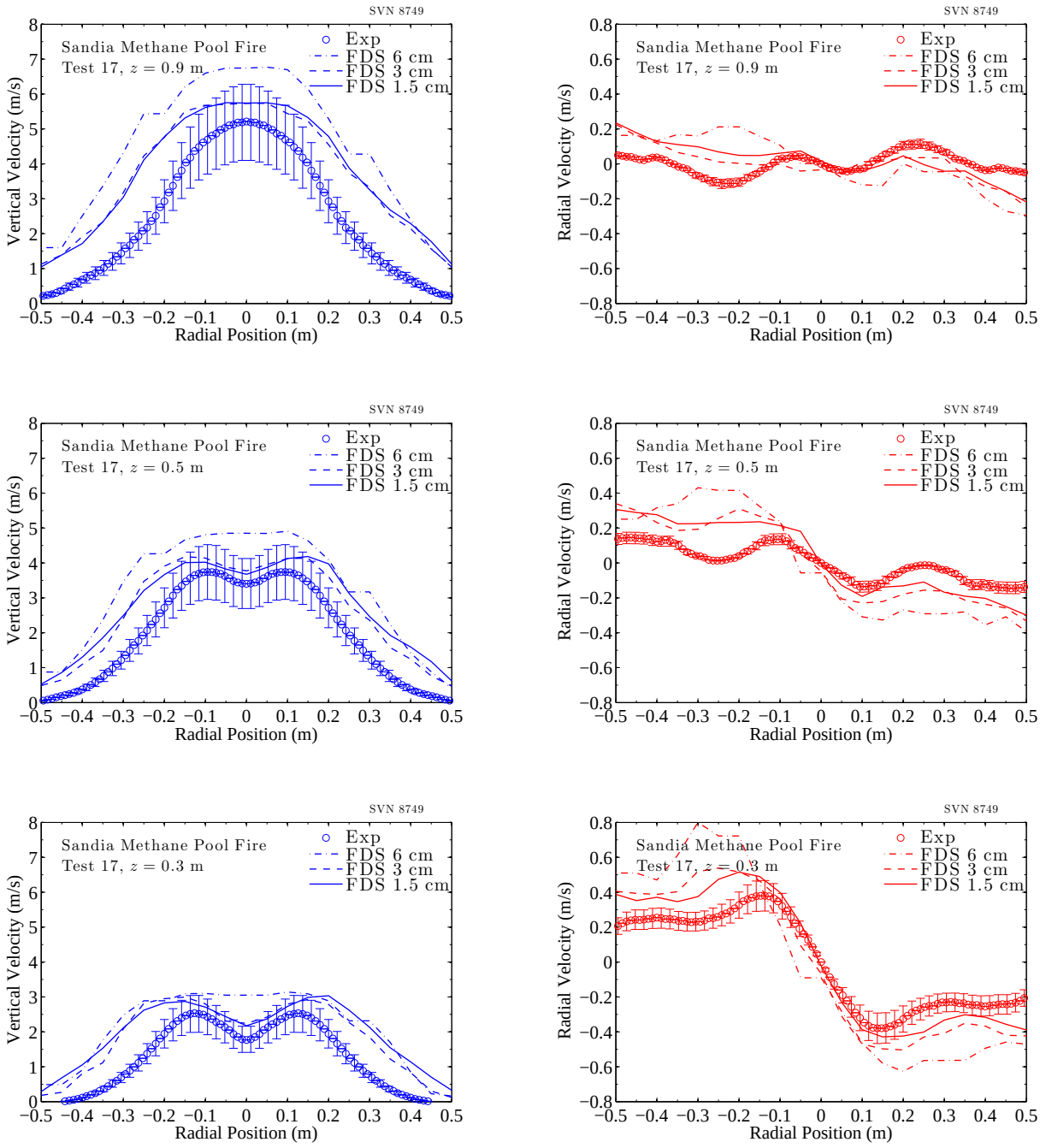

Figure 13: FDS predictions of mean velocity profiles (left: vertical, right: radial) for the Sandia 1 m methane pool fire experiment, Test 17. Results are shown for 6 cm, 3 cm and 1.5 cm grid resolutions (respectively, $D^*/\delta x = 25, 50, 100$). The z coordinate represents height above the methane pool; bottom row: $z = 0.3$ m, middle row: $z = 0.5$ m, and top row: $z = 0.9$ m.

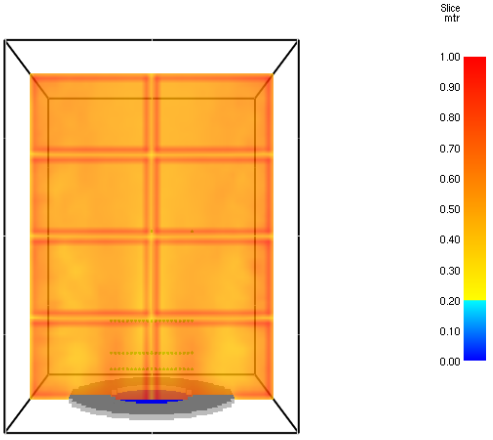

Figure 14: MTR, $\delta x = 6$ cm.

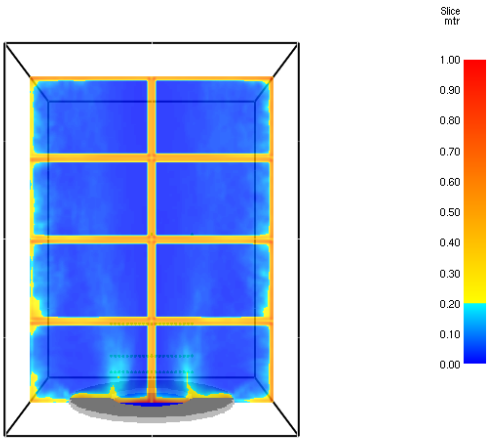

Figure 15: MTR, $\delta x = 3$ cm.

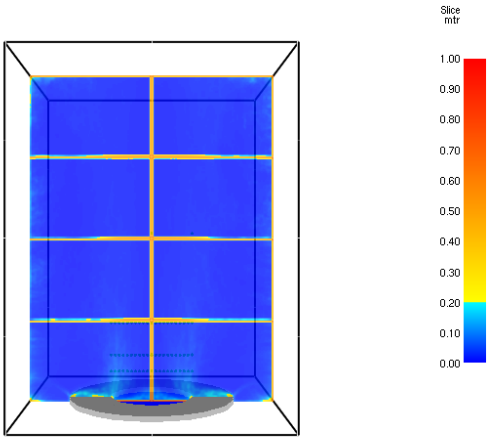

Figure 16: MTR, $\delta x = 1.5$ cm.

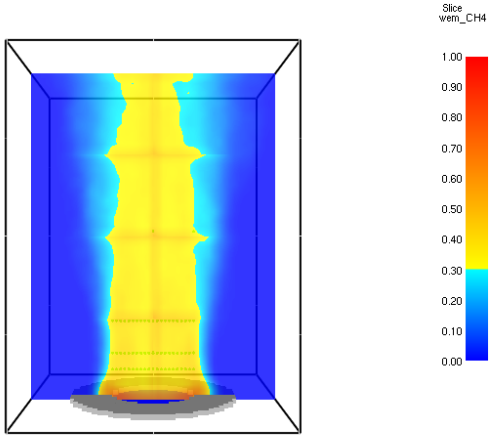

Figure 17: WEM of CH4 mass fraction, $\delta x = 6$ cm.

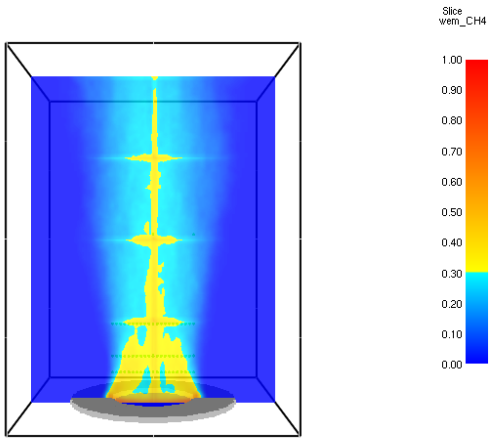

Figure 18: WEM of CH4 mass fraction, $\delta x = 3$ cm.

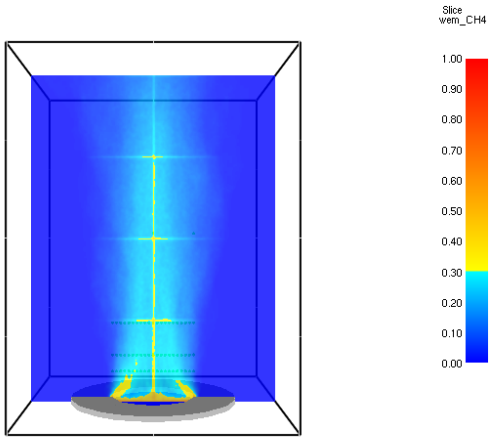

Figure 19: WEM of CH4 mass fraction, $\delta x = 1.5$ cm.